Chapter 8

Magnetic Texturing of High-T_c Superconductors

Laureline Porcar, Patricia de Rango, Daniel Bourgault and Robert Tournier

Additional information is available at the end of the chapter

http://dx.doi.org/10.5772/48698

1. Introduction

The magnetic field is an efficient tool for characterizing materials but also for elaborating them with a determined magnetic and crystallographic microstructure. The main effect of a magnetic field is to align crystallites embedded in the liquid along their easy magnetization axis [1,2]. The texturing is successful when the force exerted on the crystal gives rise to a rotation thanks to the presence of a liquid around the particle. The possibility to texture under a magnetic field is nowadays known and is still studied worldwide. However, in this paper, we aim to focus the attention on the role of the overheating above the liquidus temperature where our experiments and calculations show that nuclei are surviving above this temperature [3-7]. This assumption contradicts the classical nucleation model where intrinsic nuclei are not present above the melting temperature T_m and cannot act as growth nuclei while cooling down the temperature below T_m [8-10]. Furthermore, melts can usually be supercooled below their melting or liquidus temperatures (T_m). The degree of supercooling (ΔT-), measured by the difference between the onset temperature of solidification and T_m, is affected by various factors, including the level of overheating and the time. The relations between the overheating (ΔT+), and the supercooling (ΔT-) were studied in Sn and Sn-Pb [11].The dependence of (ΔT+) on (ΔT-) is a function of the holding time. It is well known that the cooling rate plays an important role in establishing the degree of supercooling since the nucleation of solid structures and thus solidification requires a certain period of time. Reversibly, melting also takes a certain period of time to destroy the order structures. Furthermore, it is worth noting that as long as some residual solid particles (nuclei) exist above the melting temperature, the energy barrier for the nucleation of crystallization during cooling can be reduced and thus the level of supercooling will be nil. As soon as the solid structures in the melt are completely destroyed, a substantial surface energy barrier exists for the nucleation of solid particles upon cooling. Consequently, each supercooling temperature can be associated with a nucleation time. In congruent material, such as Bi, only few crystals are obtained after an overheating of 80°C [1,7]. Then, the magnetic field can act on these remaining nuclei embedded in the liquid above the melting point.

The magnetic field was successfully used to improve texturing in crystals and alloys. The texturing of several alloys under a magnetic field was carefully studied [12]. It depends on the magnetic properties of the crystallizing nuclei and those of the melt. The mechanical force moment allowing the rotation of crystals along the direction of the magnetic field also depends on the degree of homogeneity of the magnetic field. In a homogeneous field, the texture can be induced in a magnetic isotropic crystal due to the moment of forces deriving from the demagnetizing factor and the shape anisotropy of the nucleus. However, at high temperatures and for low susceptibility, this contribution will be neglected. On the contrary, in an anisotropic crystal, the orientation arises from the anisotropic crystal characterized by an difference of magnetic susceptibility $\Delta\chi$ along two mutually perpendicular axes and the moment of forces can be expressed as:

$$K = \frac{\Delta\chi}{2\mu_0} B^2 V sin2\alpha \quad (1)$$

where α is the angle between B and the axis with maximum $|\chi|$. Under real conditions, there will be a competition between magnetic orientation forces, viscous forces, convective flows in the melt and interactions between crystals or interaction with the crucible. In some cases, the orienting effect may be limited or even negligible. The window in which the orientation can be induced must be carefully found. For an alloy, Mikelson and al. found that the temperature interval in which the orienting actions of the magnetic field are effective lies below the liquidus line and to 20% of the crystallization interval.

In this article, we will focus on the texturing of high-T_c superconductors under a magnetic field where the main conditions exposed below are taken into account. The main difficulties of superconductors texturing reside in a non congruent melting of the compounds. It is the limiting factor of overheating since the phase diagram is generally complex involving a lot of transformations even above the liquidus temperature. A large overheating above the liquidus will usually lead to the formation of unwanted secondary phases during crystallization and prevent the recombination of the superconducting phase. The latter is usually taken as the critical value for the limit of overheating. The texturing under a magnetic field consist of finding the interval of overheating temperatures preventing the transformation of superconducting-phase nuclei in secondary phases and allowing a sufficient amount of liquid. Usually, the allowable overheating is a dozen of degrees above the melting temperature [7]. As will be shown below, this amount of applied overheating does not destroy the presence of nuclei.

2. Magnetic texturing

2.1. Case of $Y_1Ba_2Cu_3O_{7-\delta}$

Rare earth-$Ba_2Cu_3O_{7-\delta}$ crystals are aligned in a magnetic field at room temperature [13] and also when they are imbedded in liquid silver at high temperature [14]. A sufficient paramagnetic anisotropy remains at temperature superior to 1000 °C and the residual anisotropy energy of the crystals is larger than the energy associated with thermal

disordering effects [15]. As mentioned previously, the anisotropy energy must also compensate the viscous force in the surrounding liquid where the crystal is free to rotate in a liquid with low resistance. The temperature window inducing a magnetic orientation lies between 1040°C and 1060°C under atmospheric pressure of O_2. Below 1040°C, a solid matrix made up of $Y_1Ba_2Cu_3O_{7-\delta}$ (Y123) and $Y_2Ba_1Cu_1O_5$ (Y211) remains throughout the annealing treatment while the melting of Y123 above 1040°C leads to a liquid containing precipitates of Y211. Grains containing inclusions of this secondary phase are partially aligned below 1040 °C with their ab-plane perpendicular to the direction of the annealing field, indicating that a partial melting of the precursor takes place during processing. Both X-ray and magnetization reveal that a weak orientation occurs. For samples prepared at temperature above 1040°C, the texturing is very efficient. The sample is cut and oriented to reveal faces perpendicular to the direction of the magnetic field. X-ray spectrum is taken as a first indication of the orientation. A measure of the orientation P_{001} is given in Figure 1 as a function of annealing temperature [16].

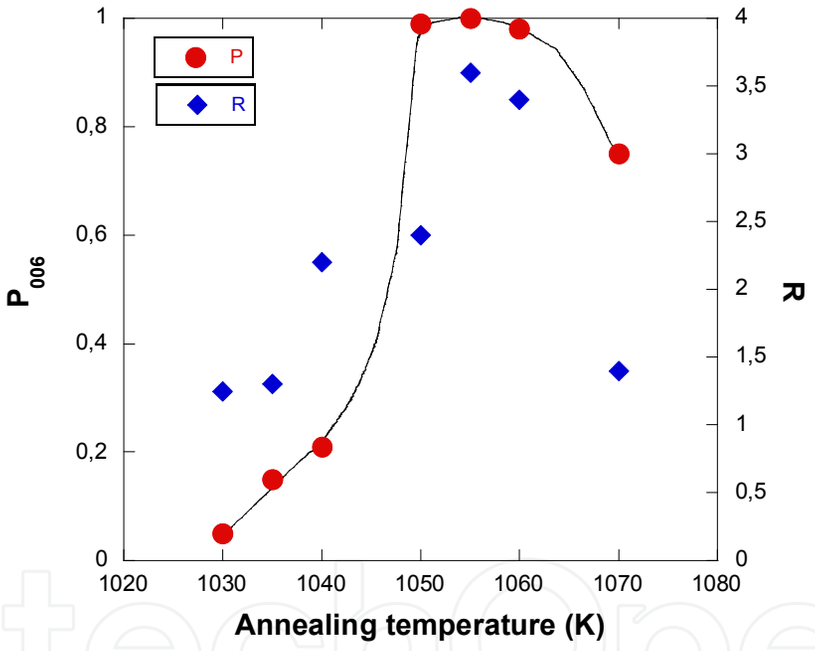

Figure 1. R and P versus annealing temperature in $Y_1Ba_2Cu_3O_{7-\delta}$ bulk textured sample, where $R=\Delta M_{H//HA}/\Delta M_{H\perp HA}$ ($\Delta M=M^+-M^-$ is the hysteresis in the sample magnetization, M^+ and M^- the values of the magnetization measured in an increasing and decreasing field respectively) and $P_{001}=1-\Gamma$ where $\Gamma=(I_{hkl}/I_{001})^o/(I_{hkl}/I_{001})^u$. I_{hkl} is the intensity of the strongest forbidden non-(00l)line and I_{001} the intensity of a (00l) line in a X-ray diffraction spectrum. The superscripts o and u indicate that measurements were performed on oriented and unoriented samples respectively [16].

In Figure 1, one can note the sharp increase of the orientation for a temperature above 1040°C while the latter gradually decreases above 1050°C. The orientation is deduced from the comparison of R, the hysteresis in sample magnetization ratio between parallel and perpendicular field. $R=\Delta M_{H//HA}/\Delta M_{H\perp HA}$ and $\Delta M=M^+-M^-$ is the hysteresis in the sample magnetization where M^+ and M^- are the values of the magnetization measured in an

increasing and decreasing field respectively. Large samples can be oriented by magnetic texturing. Superconducting critical current properties of such bulk materials were studied [17-20]. The irreversible magnetization data also indicates steady improvement in the superconducting properties of the material with increasing annealing temperature up to 1055°C. The induced orientation within the sample is directly dependent on the magnetic field value as shown in Figure 2. In order to obtain a large degree of induced anisotropy, the magnetic field must be applied continuously in the appropriate temperature regime (from the maximal temperature down to a temperature below the liquidus line), during which crystals are still free to rotate. Steady increase in the induced anisotropy is observed when the magnetic field is increased.

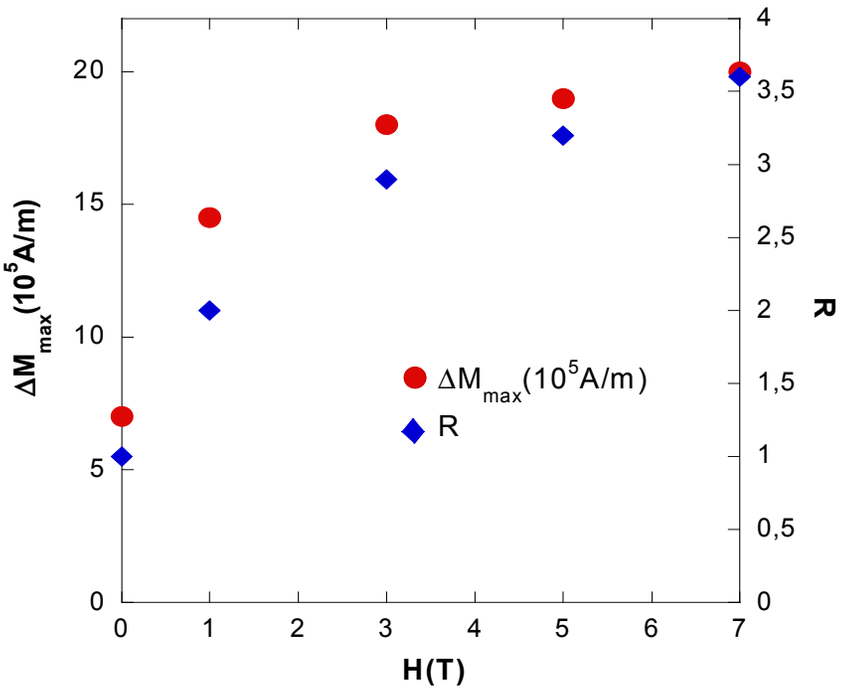

Figure 2. Variation in the magnitude of the magnetization hysteresis ΔM_{max}(●) and the ratio R(◊) with the strength of the annealing field at T_A=1055°C in $Y_1Ba_2Cu_3O_{7-\delta}$ bulk textured sample. The magnetic field was applied at all temperatures above 800°C [16].

It was also shown that the magnetic force exerted on a sample ($m\chi H_a \times dH_a/dz$) placed in a field gradient (dH_a/dz) allows the measurement of the magnetic susceptibility via the weight measurement on an electronic balance. The resulting curves provide information on the fusion, the solidification and the oxygen exchange. A typical curve presenting the magnetic susceptibility variations corrected from the oxygen weight change as a function of temperature is given in Figure 3.

When the sample is heated, the susceptibility first decreases following a Curie law behavior. When Y123 melts, between 1000 °C and 1040°C, the susceptibility increases because the melt is more paramagnetic than the phase. In the liquid state, above 1040°C, the oxygen stoichiometry changes and the mean ratio of copper valence is changed in the melt. The magnetic Cu^{2+} ions are progressively reduced in non-magnetic ions Cu^{+} through the reaction

: $2CuO \rightarrow Cu_2O + 1/2O_2$ resulting in a rapid decrease of the susceptibility. When the reduction of the magnetic copper is taken into account via the mole fraction loss of oxygen, the susceptibility corrected obeys a classical Curie law as a function of temperature. Consequently above 1070°C, largely above the peritectic temperature, the nuclei composition changes since the melt is transformed and non-superconducting nuclei of secondary phases appear. It is the reason why the magnetic field is no more effective at very high temperature. The value of the supercooling can also be measured while cooling down.

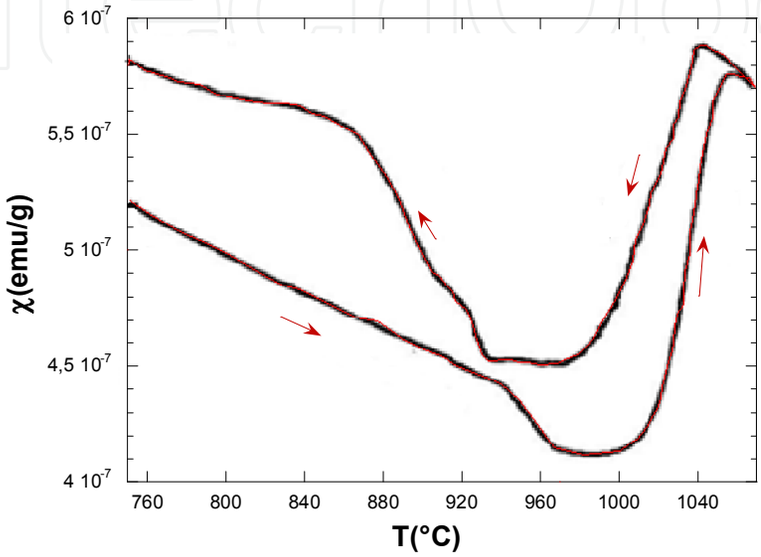

Figure 3. Magnetic susceptibility χ of $Y_1Ba_2Cu_3O_{7-\delta}$ at high temperature. Usually a change in the slope is attributed to a change of phase or to a change in composition.

Nowadays, top-seed melt texturing is mainly used to texture Y123 pellet where the crystallographic orientation is given by the crystal seed. The largest intrinsic nuclei which are involved in magnetic texturing are melted with an overheating temperature of about 1080 °C in order to be sure that crystallization is induced by the seed and not by intrinsic nuclei. In this technique, the growth of a main Y123 grain starts from a seed which has a higher peritectic decomposition temperature and crystallographic parameters close to Y-123. Pellets up to 10 cm of diameter were grown with this technique [21].

2.2. Case of $Bi_2Sr_2CaCu_2O_{8+x}$

2.2.1. Pellets of $Bi_2Sr_2CaCu_2O_{8+x}$

In $Bi_2Sr_2CaCu_2O_{8+x}$ (Bi2212), the achievement of the primary phase after melting is not easy. The system Bi_2O_3-SrO-CaO-CuO is composed of 4 elements. The phase equilibrium is complex and the recombination of the primary phase from the melt is not always reversible when the composition in the liquid is too much changed. Small variations of composition or temperature induce large changes in the equilibrium and distributions of phases. Bi2212 phase can be in equilibrium with most of the system composites Bi_2O_3-SrO-CaO-CuO. Up to fifteen four-phase equilibriums were mentioned in the literature. The melting give rises to

secondary non-superconducting phases that are not entirely consumed during solidification. There is a change in the liquid structure about 30 °C above the melting temperature of Bi2212 and Bi2223 in air as shown in Figure 4. [22,23]. The solidification of Bi2212 from the melt requires a precise control of the temperature and composition.

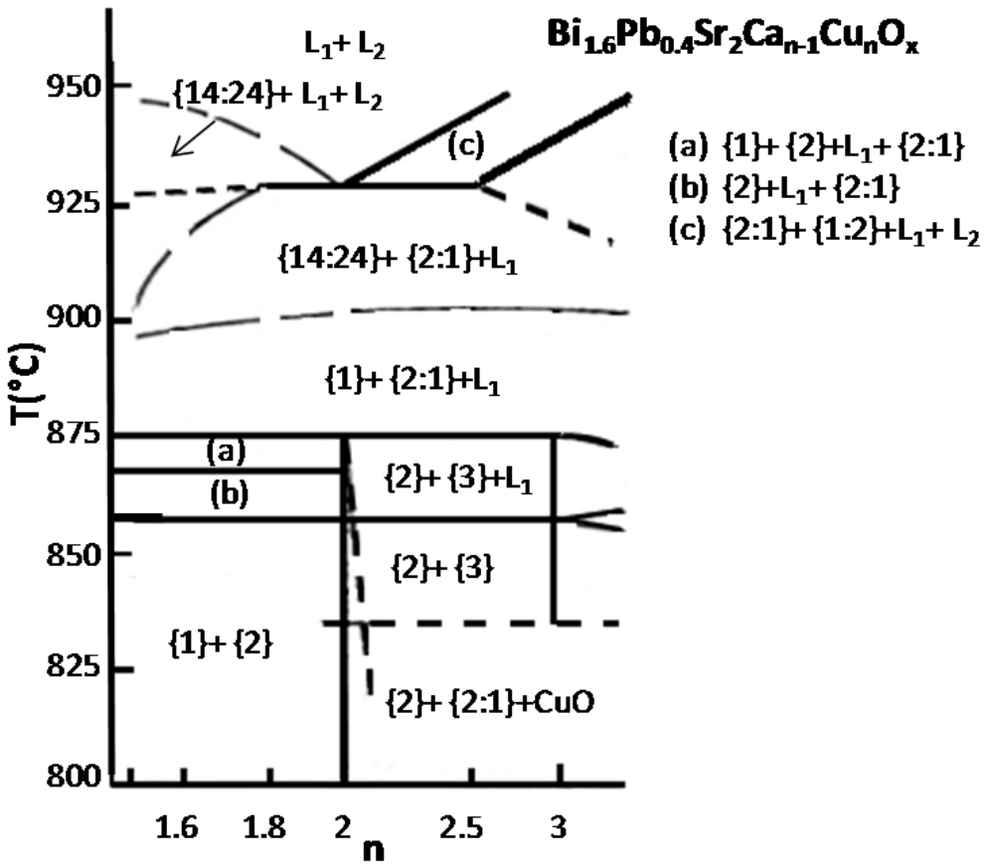

Figure 4. Part of the phase diagram of $Bi_{1.6}Pb_{0.4}Sr_2Ca_{n-1}Cu_nO_x$ as described in [23] for n varying between 1.5 and 3 and temperatures between 800 and 950°C.Phase {1} $Bi_2Sr_2Ca_0Cu_1O_x$ (n=1) ; phase {2} $Bi_2Sr_2Ca_1Cu_2O_x$ (n=2) ; phase {3} $Bi_2Sr_2Ca_2Cu_3O_x$ (n=3); phase {2:1} $(Sr,Ca)_2Cu_1$;phase {14:24} $(Sr,Ca)_{14}Cu_{24}$; phase {1:2} $(Sr,Ca)_1Cu_2$.

In BSSCO bulk compounds, several methods can be used and eventually mixed to induce alignment in the c-axis and overcome weak links. The magnetic field was successfully applied in this compound and important critical current densities were obtained [24-27]. A technique combining magnetic melt processing and hot forging was developed to improve the critical current densities in Bi2212 [28]. The magnetic field acts as an orienting tool while the pressing reinforces the orientation and the density. The addition of MgO in Bi2212 allows the material to keep high viscosity in the melt state at high temperature, making it compatible with a magnetic field texturing followed by hot forging. Moreover the MgO or Ag addition induces an improvement of superconducting properties.

Bi2212 powder added with 10 wt.% MgO is used as a starting powder. This mixture is cold pressed under an uniaxial pressure of 1 GPa in 20-mm diameter pellet with a thickness of 5

to 7 mm. The sample is melt-processed in a furnace inserted in the room temperature bore of a magnet. The melting temperature is determined by measuring the magnetic susceptibility as a function of temperature [6, 24,28].

The study of the magnetic susceptibility represented as a function of temperature in Figure 5 indicates the beginning of the melting process at 877°C and the end of the decomposition of the Bi2212 phases at 905°C [24]. Above 905°C, the liquid composition is stable and no phase is transformed so the magnetic susceptibility follows the classical Curie law and is proportional to 1/T. At 905°C, formation of the phases CuO and (Sr,Ca)O are observed. When the temperature is decreased, the susceptibility first increases before reaching a plateau. The beginning of the solidification can be seen when χ suddenly decreases. During cooling, the phase transformation at 740°C can be noted on the graph and corresponds to the solidification of the eutectic $Cu_2O/(Sr,Ca)_3Bi_2O_6$. In the inset figures, the susceptibility cycle was done for different maximal temperatures. One can observe that the susceptibility plateau is reached only for a maximal temperature of 892°C. Below 871°C, the susceptibility decreases during the cooling because the solidification process immediately takes place. The overheating temperature is not large enough in the interval 877-892°C. When the temperature is superior to 892°C, the susceptibility will reach the plateau before decreasing at the solidification. The liquidus temperature is equal to 892 °C [6].

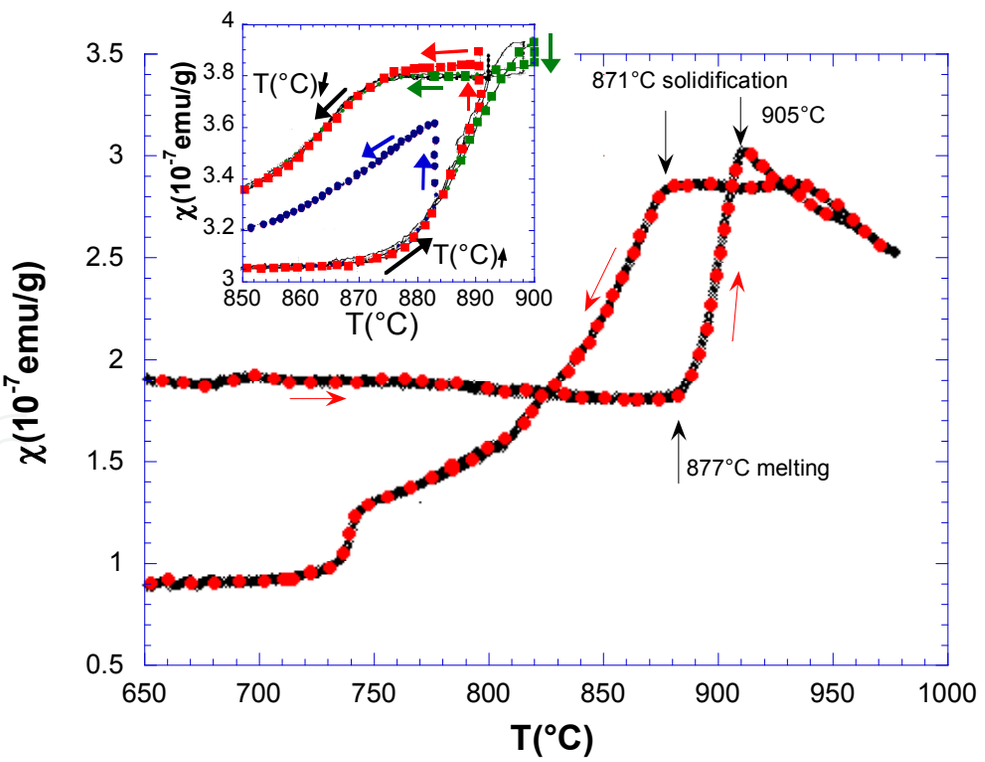

Figure 5. Magnetic susceptibility of $Bi_2Sr_2CaCu_2O_{8+x}$ at high temperature. Inset: magnetic susceptibility for different maximal temperatures. When the maximal temperature reached is inferior to 892°C, the magnetic susceptibility χ decreases during cooling. When the temperature reached is superior to 892°C, the susceptibility is first constant during cooling before decreasing [24].

The melting temperature being defined, the process can be optimized. In the process, the temperature can reach 1100°C and the vertical magnetic field used was 5.7 Tesla. The maximal processing temperature of 892°C was consequently defined as the optimum annealing temperature. Hot forging can be applied to bulk Bi2212/MgO magnetic melt processed. Hot Forging at 25 MPa during 2 hours at 880°C induces an increase in the orientation degree and of the density [28].

The magnetic melt processing performed 15°C above the onset of melting leads to the best orientation degree and thus to the best J_c. At this temperature, as was seen previously with YBaCuO the remaining magnetic susceptibility is still large enough to overcome the thermal disordering effect and there is enough liquid to allow free rotation of the crystallites. The anisotropy of susceptibility at 800 °C is equal to 4×10^{-8} emu/g [6]. For a magnetic field of 5.7T, and a temperature of 800°C, the crystals which are aligned in magnetic fields below 892 °C are larger than $10^{-21}m^3$ as determined by (1). Above this temperature, the texture is gradually lost because of the transformation of Bi2212 nuclei in secondary phases leading to a difficulty in recombining the 2212 phase.

The results are consistent with the one of H. Maeda et al. where Bi2212 bulks and tapes were processed by the MMP in magnetic fields up to 15 T following the heat treatment shown in figure 6 [26]. A texture is also developed due to the anisotropy of magnetic susceptibility. The degree of texture and the anisotropy factor in magnetization increase almost linearly with the magnetic field strength during MMP. The anisotropy factor in magnetization reaches 3.2 and 6.5 at 13 T in Bi(Pb)2212 bulks and Ag-doped Bi2212 bulks respectively. For bulk materials, the doping of some fine particles, which induce melting and crystal nucleation, is required to achieve highly textured structures by MMP. The transport critical current density J_c and the transport critical current I_c of Bi2212 tapes increase with increasing Ha due to the texture development. These results indicate that MMP is effective to enhance the texture development and J_c values for Bi2212 bulks and tapes with thick cores, making it possible to fabricate tapes with high I_c.

These observations are also consistent with the fact that above the melting point, remaining nuclei subsist that tend to be aligned in the direction of the magnetic field when they are cooled in the window of solidification. However, leaving aside the difficulty to form different phases and to lose the initial composition when the overheating is too large, exceeding too much the melting temperature reduces the presence of the intrinsic nuclei which cannot act as growth crystals during solidification and the orientation and texture are progressively lost when the temperature is 30 °C above 892 °C.

2.2.2. Ag-sheated tapes of $Bi_2Sr_2CaCu_2O_{8+x}$

Magnetic texturing of Ag-sheathed tapes was studied in very high fields and lead to high critical current densities [27,29-32]. E. Flahaut demonstrated in his PhD the possibility to texture highly homogeneous Bi2212 tapes by moving the tape in the furnace and using a continuous melting process with large critical currents (J_c = 230kA/cm² at 4.2K, self field) [33].

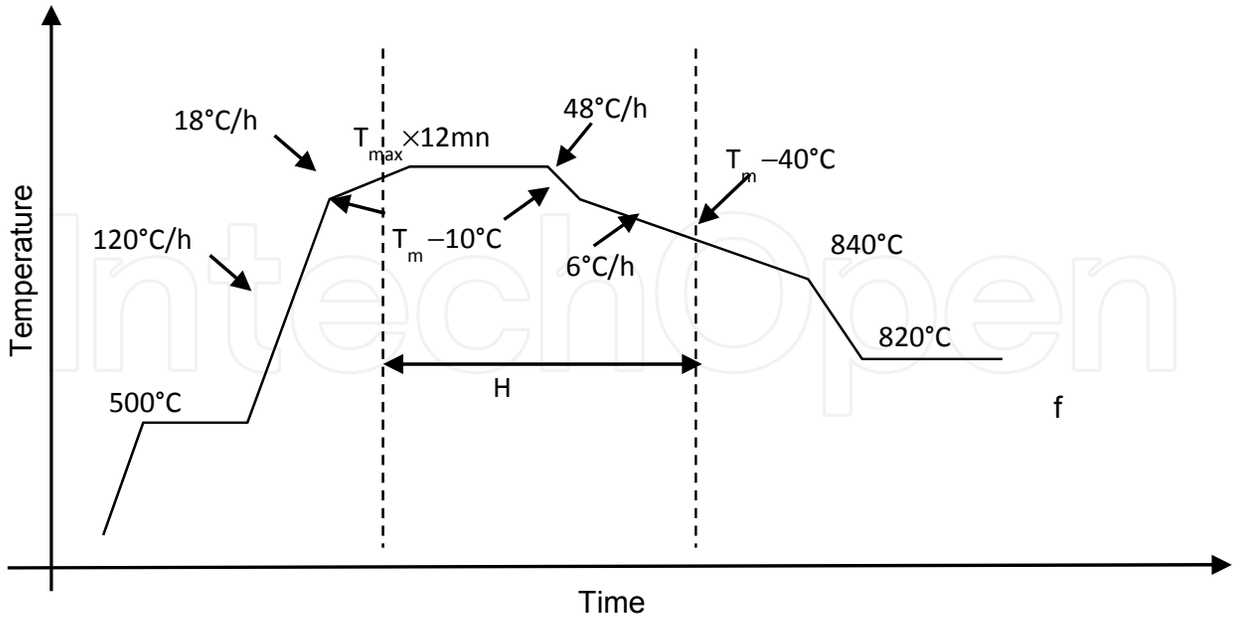

Figure 6. Generalized temperature profile for MMP $Bi_2Sr_2CaCu_2O_{8+x}$ tapes in magnetic field up to 15T [26]. T_{max} is the maximal annealing temperature. The magnetic field is applied at T_{max} and shut down at T_{max} - 40°C. The atmosphere is flowing O_2.

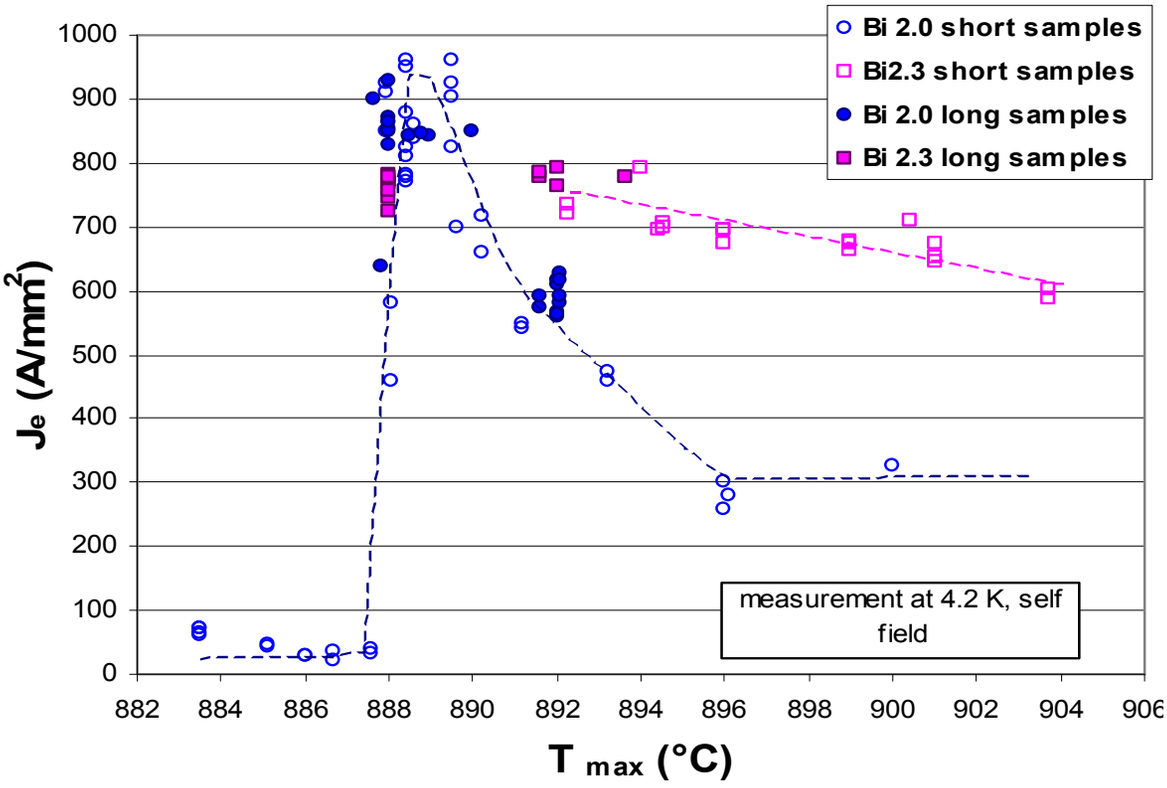

Figure 7. Critical current density in $Bi_2Sr_2CaCu_2O_{8+x}$ Ag-sheathed tapes as a function of maximal temperatures [34] for two different compositions. Pre-reacted $Bi_2Sr_2CaCu_2O_{8+x}$ powders are used.

It was shown that the critical current density can be improved with this method compared to a standard static heat treatment. The continuous process is applied to the fusion stage, the most sensitive treatment where the temperature must be carefully controlled, in order to improve the homogeneity of the sample. There are two reasons why a continuous process improves the critical current. Firstly, it allows the whole tape to be subjected to the same maximal temperature which is not the case in a furnace where the temperature must be perfectly homogeneous along the sample volume. Secondly, the texture can be improved by the thermal gradient that induces an orientation of the crystallites along the silver sheath of each filament. The engineering critical current density of Bi2212 tapes at 4.2K is plotted as a function of maximum annealing temperature used in the melting process in figure 7 [34]. The critical current is measured by a classical four point method. It is a good representation of the superconducting and crystallographic properties of the samples. Usually, a poor critical current is coming from a poor connectivity between the grains resulting from a lack of orientation and accumulation of secondary phases at the grain boundaries. The critical current density is maximal at the melting temperature and in a very narrow window of temperatures above the melting temperature. The Bi2212 nuclei acting in the magnetic texturing are also present in the narrow sheaths and induce the crystal growth. When the overheating temperature is too large, the critical current density progressively decreases for all the reasons mentioned above.

2.2.3. Magnetic field texturing of 2212 tapes using a continuous displacement in the furnace

Bi2212 multifilament tapes were processed by the well-established powder-in-tube (PIT) technique. The tape is composed of 78 filaments embedded in a Ag–Mg (0.2% Mg) sheath [35]. The tapes are different from the ones before. A dynamic heating process was inserted into a superconducting coil to enable a dynamic heat treatment under a magnetic field (5 T) in order to obtain homogeneous and high critical current densities (figure 8).

The thermal treatment consists in a melting step for 250 s and a slow temperature decrease (0.1 °C s^{-1}). The atmosphere is 40% flowing O_2. The maximum applied field is 5T. Critical current densities in Bi2212 tapes were measured in self field at 4.2K to compare the benefit of a magnetic field during the dynamic heat treatment. An increase of the critical current density is obtained under the application of a magnetic field at T= 894 °C as can be seen in figure 9. The processing speed is around 1cm/min. The results are reproducible and this gain in current densities is observed for temperature around 894°C. The results are consistent with the ones previously presented for Y123 and Bi2212 bulk samples. The rotation of the crystallites under a magnetic field is possible when the liquid at the interface of the grains is sufficient and its viscosity is high which implies a relatively high temperature of the melt. Above 896°C, the refractory and non-superconductive phases tend to grow rapidly, limiting the critical current density. The dynamic heat treatment under a magnetic field offers several benefits. Firstly, the temperature is highly homogeneous. Secondly, no long treatments are necessary and the texture can be obtained homogenously and rapidly. This is also due to the facts that the nuclei causing the growth of the right phase subsist in the melt and don't need the recombination in the solid state that requires long time.

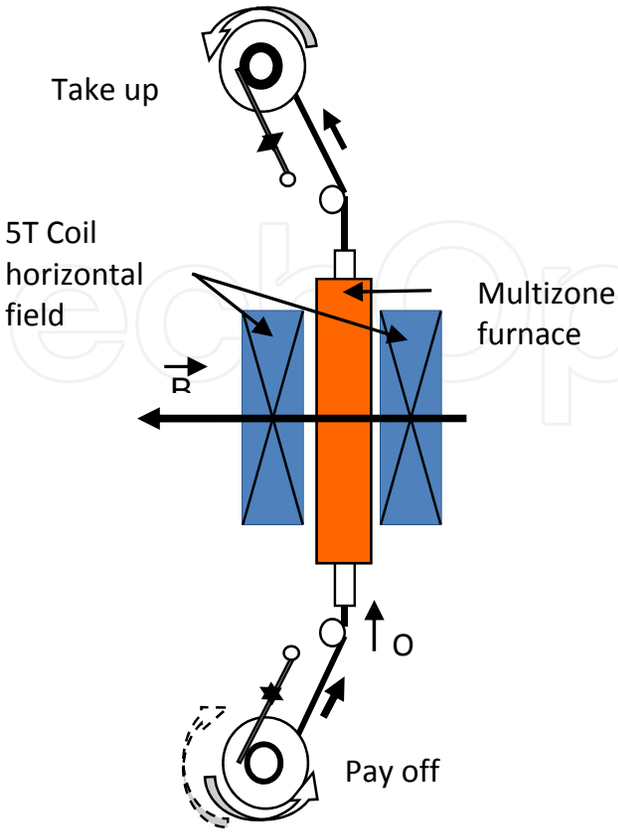

Figure 8. Dynamic heat process under a magnetic field. A multizone furnace is inserted in a superconducting coil reaching 5T. Flowing O_2, maximal temperature and processing speed are important parameters that can be controlled [35].

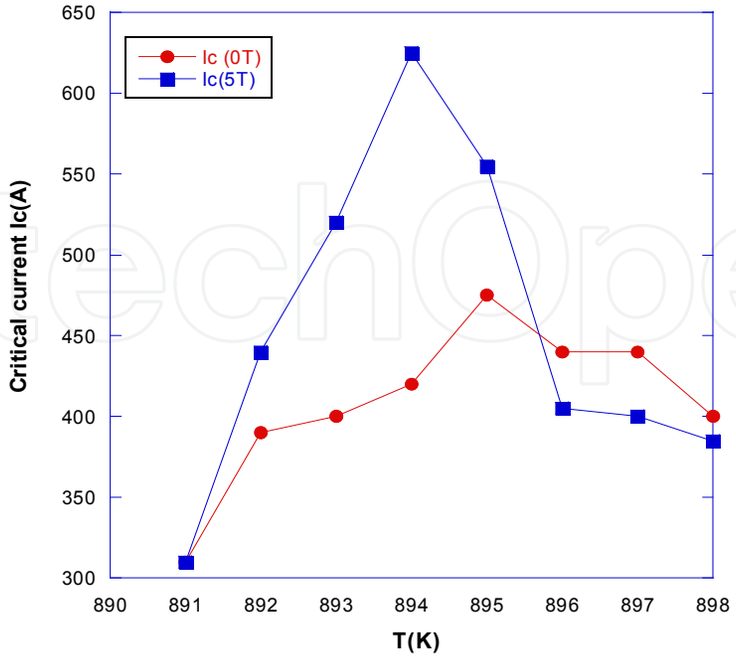

Figure 9. Critical current in Ag sheathed tapes of $Bi_2Sr_2CaCu_2O_{8+x}$ as a function of maximal annealing temperature measured at 4.2K with field and without field [35].

2.3. Case of $Bi_2Sr_2Ca_2Cu_3O_{8+x}$

2.3.1. Pellets of $Bi_2Sr_2Ca_2Cu_3O_{8+x}$

J. Noudem demonstrates the possibility to form the $Bi_2Sr_2Ca_2Cu_3O_{8+x}$ (Bi2223) phase after a liquid transformation above the melting temperature [36 - 38]. As seen previously in the Bi2212 compounds, the phase diagram is complex which requires a precise control of the temperature and composition [23].

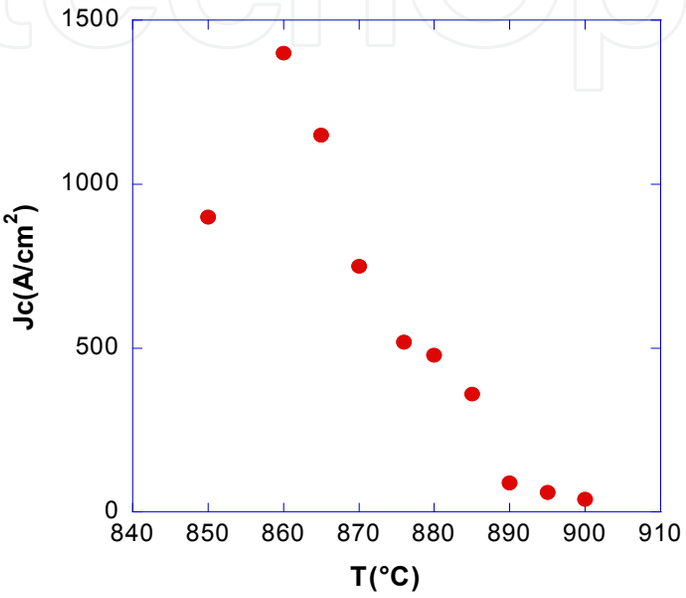

Figure 10. Critical current density in Bi2223 textured bulk compounds measured at 77K as a function of the maximal annealing temperature [38].

The texture along the c-axis is induced by means of a magnetic field. Pellets of Bi2223 were first uniaxialy pressed before annealing. The heating cycle took place in a vertical furnace placed in a superconducting magnet reaching 8T. The optimum maximum temperature lies within the range 855° and 900°C and is followed by a slow decrease in temperature of 2°C/h. A maximal value of critical current density of 1450 A/cm² was obtained for a temperature reaching 860°C during 1 hour. Below this value, the proportion of liquid phase is too small to allow rotation of the platelets under the influence of the magnetic field and the critical current consequently sharply decreases. Above this optimum processing temperature, the transformation of Bi2223 nuclei in secondary phases $(Ca/Sr)_{14}Cu_{24}O_y$, CuO and $(Ca/Sr)_2CuO_3$ prevent the recombination of Bi2223. Thus, the critical current density gradually decreased until zero around 900°C as shown in Figure 10 in agreement with the phase diagram of Figure 4.

2.3.2. Ag-sheated tapes of $Bi_2Sr_2Ca_2Cu_3O_{8+x}$

The possibility to obtain high critical current and a good homogeneity in Ag-sheathed Bi2223 tapes could follow accordingly to the previous results However, the complexity of

the Bi,Pb(2223) phase diagram and the presence of numerous secondary phases coexisting with the Bi,Pb(2223) phase as shown in Figure 4 has led to a standard route of tapes preparation where precursor powders are calcined and pre-reacted before the cold deformation inside the Ag tubes. This route implies the use of Bi2212 phase as the predominant phase and a series of cold deformations (swaging, drawing and rolling) before heat-treated the Ag-sheathed tapes to achieve Bi,Pb(2223) phase. However, intrinsic limits to this route seem to come from the formation mechanisms where the transient liquid assisting the Bi,Pb(2223) formation is not stable and results in a poor structural homogeneity. E. Giannini et al showed that it is possible to form the Bi,Pb(2223) phase from a liquid close to the equilibrium conditions following a reversible melting of the Bi,Pb(2223) phase exactly in the same way as J. Noudem et al. did in bulk samples [39]. Then, Bi2223 intrinsic nuclei exist in the melt. This new route is extremely sensitive to the temperature profile and is dependent of the local Pb content [40]. This result confirms the possibility to texture Ag-sheathed Bi,Pb(2223) tapes by means of a scrolling continuous heat treatment under a magnetic field.

3. Magnetic texturing induced by intrinsic growth nuclei surviving above the melting temperature

3.1. Intrinsic nuclei surviving above the melting temperature

Undercooling temperatures of liquid alloys depend on the overheating rate above the melting temperature T_m of liquid alloys and elements [41-43]. The experiments presented in section 2 lead to the conclusion that intrinsic nuclei exist above T_m and are aligned in magnetic field during the growth time evolved in the solidification window between liquidus and solidus temperatures [7]. These results are in contradiction with the idea [8-10] that all crystals have to disappear at the melting temperature T_m by surface melting. The classical equation of Gibbs free energy change associated with crystal formation also predicts that the critical radius for crystal growth becomes infinite at T_m and all crystals are expected to melt [8-10]. It has been recently proposed to add an energy saving ε_v produced by the equalization of Fermi energies of out-of-equilibrium crystals and their melt in this equation [5,6].

Transformation of liquid-solid always induces changes of the conduction electron number per volume unit, and sometimes per atom. The equalization of Fermi energies of a spherical particle having a radius R smaller than a critical value $R^*_{2ls}(\theta)$ produces an unknown energy saving $-\varepsilon_v$ per volume unit. The ε_v value is equal to a fraction ε_{ls} of the fusion heat ΔH_m per molar volume V_m. This energy was included in the classical Gibbs free energy change $\Delta G_{1ls}(\theta,R)$ associated with crystal formation in metallic melts [5,6,10]. The modified free energy change is $\Delta G_{2ls}(R,\theta)$ given by (2) and $\Delta G_{1ls}(\theta,R)$ is obtained with $\varepsilon_{ls} = 0$:

$$\Delta G_{2ls}(R,\theta) = \frac{\Delta H_m}{V_m}(\theta - \varepsilon_{ls})4\pi\frac{R^3}{3} + 4\pi R^2\frac{\Delta H_m}{V_m}(1+\varepsilon_{ls})\left(\frac{12k_B V_m \ln K_{ls}}{432\pi\times\Delta S_m}\right)^{1/3} \quad (2)$$

where ΔS_m is the molar fusion entropy, $\theta = (T-T_m)/T_m$ the reduced temperature, R the growth nucleus radius, $\varepsilon_{ls} \times \Delta H_m/V_m$ the energy saving ε_v, N_A the Avogadro number, k_B the Boltzmann constant. The $\ln K_{ls}$ given in (3) depends on the viscosity through the Vogel-Fulcher-Tammann (VFT) temperature T_{0m} of the glass-forming melt which corresponds to the free volume disappearance temperature [44,45]:

$$\ln(K_{lgs}) = \ln(\frac{A\eta_0}{\eta}) = (\ln A) \pm 2 - \frac{B}{(T - T_{0m})} \tag{3}$$

where lnA is equal to 87±2, $B/(T_g-T_{0m})$ = 36-39, T_g being the vitreous transition temperature [46,47]. The critical radius and the critical energy barrier are respectively given versus temperature by (4) and (5) assuming that a minimum value of ε_v exists at each temperature $T \le T_m$ and $\varepsilon_{ls} = 0$ for $R > R^*_{2ls}$:

$$R^*_{2ls}(\theta) = \frac{-2(1+\varepsilon_{ls})}{\theta - \varepsilon_{ls}} (\frac{V_m}{N_A})^{1/3} (\frac{12 k_B N_A \ln K_{ls}}{432\pi \times \Delta S_m})^{1/3} \tag{4}$$

$$\frac{\Delta G^*_{2ls}}{k_B T} = \frac{12(1+\varepsilon_{ls})^3 \ln K_{ls}}{81(\theta - \varepsilon_{ls})^2 (1+\theta)} \tag{5}$$

The critical radius at the melting temperature is no longer infinite at T_m ($\theta = 0$) because ε_{ls0} is not nil. Out-of-equilibrium crystals having a radius smaller than R^*_{2ls} are not melted because their surface energy barrier is too high. The thermal variation of ε_{ls} is an even function of θ given by (6):

$$\varepsilon_v = \varepsilon_{ls} \frac{\Delta H_m}{V_m} = \varepsilon_{ls0} (1 - \frac{\theta^2}{\theta^2_{0m}}) \frac{\Delta H_m}{V_m} \tag{6}$$

where θ_{0m} corresponds to the free-volume disappearance temperature T_{0m} [5]. The fusion entropy is always equal to the one of the bulk material regardless of the crystal radius R and of ε_{ls0} value as shown in (7) because $d\varepsilon_{ls}/dT = 0$ at the melting temperature T_m of the crystal :

$$\frac{3}{4\pi R^3} \left\{ \frac{d\left[\Delta G_{2ls}(\theta)\right]}{dT} \right\}_{T=T_{mc}} = -\frac{\Delta S_m}{V_m} \tag{7}$$

All crystals outside a melt generally have a fusion temperature depending on their radius; they melt by surface melting. Here, they melt by homogeneous nucleation of liquid droplets. These properties are analogous to that of liquid droplets coated by solid layers that are known to survive above T_m [48,49]. The crystal stability could be enhanced by an interface thickness of several atom layers [50] or these entities could be super-clusters which could contain magic numbers of atoms [51,52]. They could melt by liquid homogeneous nucleation instead of surface melting. The presence of super-clusters in melts being able to act as growth nuclei was recently confirmed by simulation and observation in glass-forming melts and liquid elements [53-55].

The equalization of Fermi energies of out-of-equilibrium crystals and melts does not produce any charge screening induced by a transfer of electrons from the crystal to the melt as assumed in the past [5,6,47]. It is realized by a Laplace pressure p given by (8) [56,57] depending on the critical radius R^*_{2ls} and the surface energy σ defined by the coefficient of $4\pi R^2$ in (2):

$$p = \frac{2\times\sigma}{R^*_{2ls}} = \frac{\Delta H_m}{V_m}[\theta - \varepsilon_{ls}(\theta)] \tag{8}$$

The energy saving coefficient ε_{ls} and consequently p can be determined from the knowledge of the vitreous transition T^*_g in metallic and non-metallic glass-forming melts [56,57]. The liquid-glass transformation is accompanied by a weakening of the free volume disappearance temperatures from θ_{0m} to θ_{0g}, of energy saving coefficients at T_m from ε_{ls0} to ε_{lg0} and consequently of VFT temperatures from T_{0m} to T_{0g} [56]. The vitreous transition T^*_g occurs at a crystal homogeneous nucleation temperature T_{2lg} giving rise, in a first step, to vitreous clusters during a transient nucleation time equal to the glass relaxation time. The energy saving coefficients ε_{ls0} and ε_{lg0} are determined by θ^*_g respectively given by (9) and (10):

$$\varepsilon_{lg0} = \varepsilon_{lg}(\theta = 0) = 1.5 * \theta^*_g + 2 \tag{9}$$

$$\varepsilon_{ls0} = \varepsilon_{ls}(\theta = 0) = \theta^*_g + 2 \tag{10}$$

The free-volume disappearance reduced temperature θ_{0m} of the melt above T^*_g which is equal to its VFT temperature [45] is given by (11)]:

$$\theta^2_{0m} = \frac{8}{9}\varepsilon_{ls0} - \frac{4}{9}\varepsilon^2_{ls0} \tag{11}$$

These formulae are applied to Bi2212 with $\theta^*_g = -0.42$ ($T^*_g = 676$ K); T^*_g is assumed to be 50 K below the first-crystallization temperature observed at 723 K [58]. Using (10), we find $\varepsilon_{ls0} = 1.58$ and $T_{0m} = 532$ K with a liquidus temperature of 1165 K [59]. The $\ln K_{ls}$ is equal to 76.4 with lnA = 85 and $B/(T_m\text{-}T_{0m}) = 8.6$. The fusion heat ΔH_m is chosen to be equal to the mean value of 11 measurements depending on composition minus the heat produced by an oxygen loss of 1/3×mole [22,25,60]. We obtain $\Delta H_m = 7100 - 2000 = 5100$ J/at.g, a molar volume $V_m = 144*10^{-6}$ m^3 and a fusion entropy 4.38 J/K/at.g. Another evaluation of ΔH_m leads to 4600 J using a measured oxygen loss of 2.1% of the sample mass in a magnetic field gradient maximum at the liquidus temperature T = 1165 K and a measured heat of 8000 J/at.g for a composition 2212 [60]. The critical radius R^*_{2ls} ($\theta = 0$) in the two cases are respectively equal to 8.94×10^{-10} and 9.27×10^{-10} m; these critical nuclei contain 188 and 209 atoms (Bi, Sr, Ca, Cu and O). Surviving nuclei have a smaller radius and contain less atoms. The energy saving coefficient ε_{nm0} of non-melted crystals has to be determined in order to explain why growth nuclei are of the order of 10^{24}-10^{25} per m^3 as shown by nano-crystallization of glass-forming melts and are able to induce solidification at T_m when the applied overheating rate remains weak [47,61].

3.2. Melting temperature of surviving intrinsic nuclei as a function of their radius

The radius R of liquid droplets which are created by homogeneous nucleation inside an out-of-equilibrium crystal of radius R_{nm} as a function of the overheating rate θ is calculated from the value of ΔG_{2sl} given by (12); (12) is obtained by replacing θ by –θ in (2) because the transformation occurs now from crystal to melt instead of melt to crystal:

$$\Delta G_{2sl}(R,\theta) = \frac{\Delta H_m}{V_m}(-\theta - \varepsilon_{nm0})4\pi\frac{R^3}{3} + 4\pi R^2\frac{\Delta H_m}{V_m}(1+\varepsilon_{nm0})\left(\frac{12k_B V_m \ln K_{ls}}{432\pi\times\Delta S_m}\right)^{1/3} \quad (12)$$

where ε_{ls} given by (6) is replaced by ε_{nm0} when $\theta \geq 0$ because the Fermi energy difference between crystal and melt is assumed to stay constant above T_m. A crystal melts at $T > T_m$ when its radius R_{nm} is smaller than the critical values 0.894 or 0.927 nm. The equation (13) of liquid homogeneous nucleation in crystals with the nucleation rate $J = (1/v.t_{sn})$ is used to determine $\Delta G_{2sl}/k_BT$ as a function of R_{nm} [7,10,47,62]:

$$\ln(J.v.t_{sn}) = \ln(K_{sl}.v.t_{sn}) - \frac{\Delta G_{sl}(R_{nm},\theta)}{k_B T} = 0 \quad (13)$$

where v is the surviving crystal volume of radius R_{nm} and t_{sn} the steady-state nucleation time evolved at the overheating temperature T. The radius R_{nm} being smaller than 1 nanometer and t_{sn} chosen equal to 1800 s, $\ln(K_{sl}.v.t_{sn})$ is equal to 32-35 with $\ln K_{sl}$ being given by (3).

The equalization of Fermi energies in metallic melts is accomplished through Laplace pressure. We have imagined another way of equalizing the Fermi energies of nascent crystals and melt instead of applying a Laplace pressure [5,6,47]. Free electrons are virtually transferred from crystal to melt. The quantified energy savings of crystals having a radius R_{nm} equal or smaller than the critical value would depend on the number of transferred free electrons. A spherical attractive potential would be created and would bound these s-state conduction electrons. This assumption implies that the calculated energy saving ε_{nm0} at $T = T_m$ is quantified, depends on the crystal radius R_{nm} which corresponds to the first energy level of one s-electron moving in vacuum in the same spherical attractive potential. These quantified values of ε_{nm0} have been already used to predict the undercooling temperatures of gold and other liquid elements in perfect agreement with experiments [63,64]. As already shown, the attractive potential $-U_0$ defined by (14) is a good approximation for $n\times\Delta z >> 1$, $n = 4\pi N_A R^3/3V_m$ being the atom number per spherical crystal of radius R_{nm} and Δz the fraction of electron per atom which would be transferred in vacuum from crystal to melt, e the electron charge, $\varepsilon_{nm0}\times\Delta H_m$ the quantified electrostatic energy saving per mole at T_m, ε_0 the vacuum permittivity:

$$U_0 = \frac{n\Delta z\, e^2}{8\pi\varepsilon_0 R_{nm}} \geq E_q = \frac{n\varepsilon_{nm0}\Delta H_m}{N_A} \quad (14)$$

The potential energy U_0 is nearly equal to the quantified energy E_q with $\varepsilon_{ls0} = 1.58$ at $T = T_m$ and $\Delta z = 0.1073$ with a critical radius of 0.894 nm, $\Delta H_m = 5100$ J/atom.g, using (14). We find $\Delta z = 0.0994$ with a critical radius of 0.927 nm and $\Delta H_m = 4600$ J. Schrödinger's equation (15) is written with wave functions ψ only depending on the distance r from the potential centre for a s-state electron [65]:

$$\frac{1}{r}\frac{d^2}{dr^2}(r\psi) + k^2\psi = 0, \text{ where } k = \frac{1}{\hbar}[2m(U_0 - E_q)]^{1/2} \tag{15}$$

The quantified solutions

$$E_q = \frac{n\varepsilon_{nm0}\Delta H_m}{N_A}$$

are given by the k value and by (16) as a function of the potential U_0 associated with a crystal radius $R = R_{nm}$, n varying with the cube of R_{nm}:

$$\frac{\sin kR_{nm}}{kR_{nm}} = \frac{\hbar}{\sqrt{2mR_{nm}^2 U_0}}, \text{ where } U_0 = \frac{n\Delta z e^2}{8\pi\varepsilon_0 R_{nm}} \tag{16}$$

The quantified values of E_q at T_m and consequently of ε_{nm0} are calculated as a function of R_{nm} from the knowledge of U_o using a constant Δz. The free-energy change given by (12) is plotted versus R_{nm} in Figure 11 and corresponds to a liquid droplet formation of radius R_{nm} at various overheating rates θ. Crystals are melted when (13) is respected with $\Delta G_{2sl}/k_BT$ equal or smaller than $\ln(K_{ls}.v.t_{sn})$. All crystals having a radius larger than the critical value 0.894 nm and smaller than 0.36 nm are melted at T_m while those with $0.36 < R_{nm} < 0.894$ nm are not melted. It is predicted that, for the two ΔH_m values, they would disappear at temperatures respecting $\theta > 0.93$ assuming that all atoms are equivalent. It is known that a consistent overheating has to be applied to glass-forming melts in order to eliminate a premature crystallization during cooling [41]. A glass state is obtained when Bi-2212 melts are quenched from 1473-1523 K ($0.264 < \theta < 0.307$) after 1800 s evolved at this temperature [60,61]. Many nuclei survive after an overheating at $\theta = 0.264$. Bi2201 grains of diameter 10 nm are obtained after annealing the quenched undercooled state at 773 K during 600 s [61]. Consequently, the nuclei number is still larger than $10^{24}/m^3$ in spite of an overheating at 1473 K ($\theta = 0.264$) in agreement with the curves $\Delta G_{2sl}/k_BT$ which are larger than $\ln(K_{sl}.v.t_{sn}) \cong 20$ with t = 1800 s and $v < 1$ nm^3 .

3.3. Crystallization of melts induced by intrinsic nuclei at $T \leq T_m$

These intrinsic nuclei act as growth nuclei during a solidification process. The first-crystallization will occur when (17) will be respected at the temperature T:

$$\ln(J.v.t_{sn}) = \ln(K_{sl}.v_s.t_{sn}) - \left[\frac{\Delta G_{sl}^*(\theta)}{k_BT} - \frac{\Delta G_{nm}(\theta)}{k_BT}\right] = 0 \tag{17}$$

where $\Delta G^*_{2ls}/k_BT$ is given by (5) and $\Delta G_{nm}/k_BT$ is the contribution of unmelted crystal of radius R_{nm} to the reduction of $\Delta G^*_{2ls}/k_BT$ given by (2).

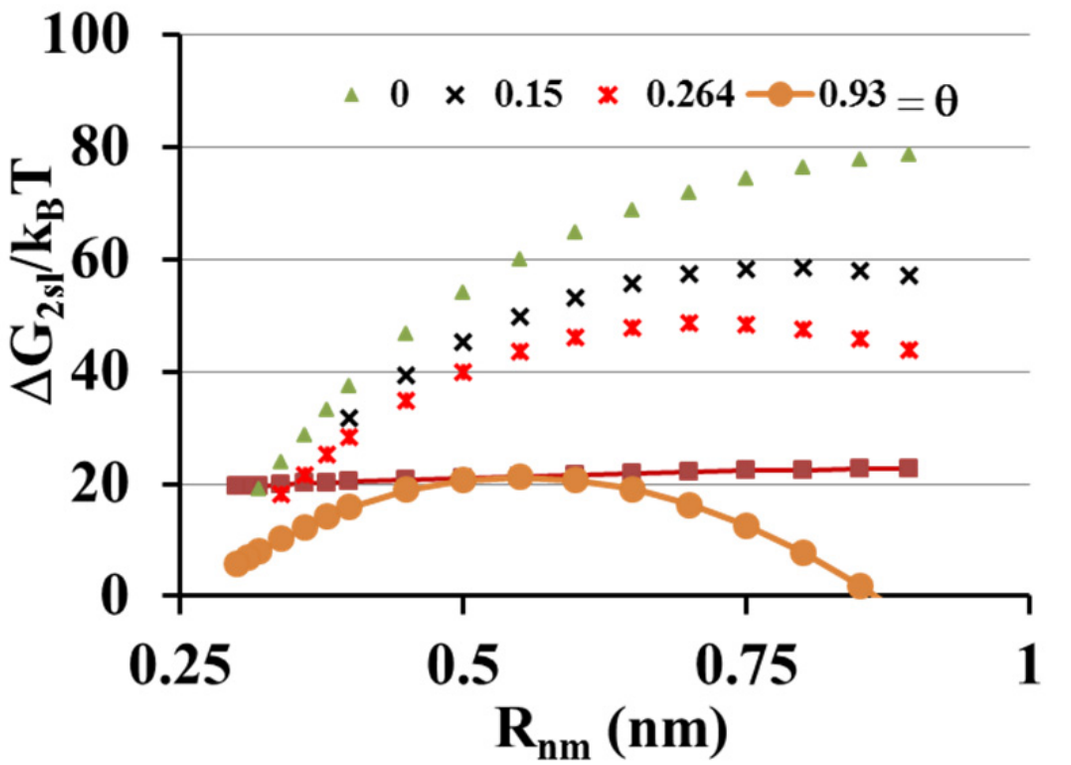

Figure 11. Values of ΔG_{2sl} given by (12) divided by k_BT and calculated with a radius R equal to an intrinsic nucleus radius R_{nm} smaller than the critical radius equal to 0.894 nanometer are plotted versus R_{nm} for $\theta = (T-T_m)/T_m = 0$, 0.1, 0.15, 0.264 and 0.93. The straight line nearly parallel to the R_{nm} axis represents $\ln(K_{ls}.v.t_{sn})$ with v equal to the volume of a sphere having a radius R_{nm}. All nuclei with $\Delta G_{2sl}/k_BT > \ln(K_{ls}.v.t_{sn})$ are not melted. The lower radius below which all nuclei melt slowly increases with θ. All nuclei would disappear after 1800 s at T = 2248 K (θ = 0.93).

The $\ln K_{ls}$ given by (3) is equal to 76.4 at T_m while the volume sample v_s is assumed to be equal to 10^{-6} and 10^{-24} m^3 respectively leading to $\ln(K_{ls}.v_s.t_{sn}) = 70.1$ and $\ln(K_{ls}.v_s.t) = 28.6$ with t_{sn} = 1800 s. In Figure 12, $(\Delta G^*_{2ls}/k_BT - \Delta G_{nm}/k_BT) = \Delta G_{eff}/k_BT$, $\ln(K_{ls}.v_s.t_{sn}) = 70.1$ and 28.6 are plotted as a function of R_{nm} at $T = T_m$. Nuclei with $0.45 < R_{nm} < 0.894$ nm could act as growth nuclei at T_m. Nuclei with R_{nm} smaller than 0.45 nm contain about one or two layers of atoms surrounding a centre atom. All metallic glass-forming melts contain the same type of clusters that govern their time-temperature-transformation (TTT) diagram above T_g [47]. The Bi2212 TTT diagram has to exist even if it is not known. In contradiction with our model of identical atoms, intrinsic nuclei having a radius R_{nm} respecting $0.45 < R_{nm} < 0.894$ nm have to be melted after an overheating up to 1473 K (θ = 0.264) because a weak cooling rate leads to a vitreous state in this type of glass-forming melt after applying an overheating rate θ = 0.264 [61].

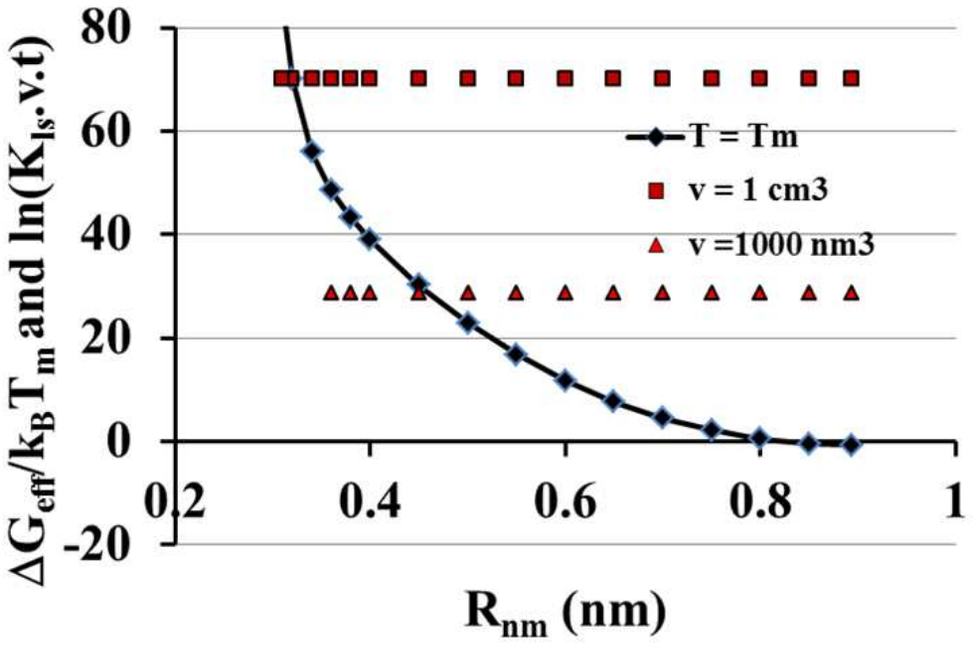

Figure 12. The difference ($\Delta G^*_{2ls}/k_BT_m - \Delta G_{nm}/k_BT_m = \Delta G_{eff}/k_BT_m$), the $\ln(K_{ls}.v_s.t) = 70.1$ with $v = 10^{-6}$ m^3, K_{ls}= 76.4, t_{sn} = 1800 s, and $\ln(K_{ls}.v.t) = 28.6$ with $K_{ls} = 76.4$, $v = 10^{-24}$ m^3 and t_{sn} = 1800 s are represented as a function of the surviving nucleus radius R_{nm}. All nuclei with $0.45 < R_{nm} < 0.894$ nm can grow at $T = T_m$ in a sample volume of 10^{-24} m^3 using our model of identical atoms.

The calculation of the first-crystallization nucleation total time t has to take into account not only the steady-state nucleation time t_{sn} but also the time-lag τ_{ns} in transient nucleation [44] with:

$$t = t_{sn} + \frac{\pi^2}{6}\tau_{ns}, \text{ when } t >> \frac{\pi^2}{6}\tau_{ns} \tag{18}$$

$$J\tau^{ns} = \frac{a_0^* N}{2\pi\Gamma}\exp(-\frac{\Delta G_{eff}^*}{k_B T}), \text{ where } \Gamma = (\frac{1}{3\pi k_B T}\frac{\Delta G_{2ls}^*}{j_c^2})^{1/2}, \ \tau^{ns} = \frac{a_0^* N}{2\pi K_{ls}\Gamma} \text{ and } j_c = \frac{32\pi\times\alpha_{2ls}^3}{3(\theta-\varepsilon_{nm})^3} \tag{19}$$

The time lag τ_{ns} is proportional to the viscosity η while the steady-state nucleation rate J is proportional to η^{-1}; the $J\tau_{ns}$ in (19) is not dependent on η [44]; Γ is the Zeldovitch factor, $a^*_0 = \pi^2/6$, N the atom number per volume unit, j_c the atom number in the critical nucleus; K_{ls} is defined by (3). Equation (17) is also applied when t_{sn} is small compared with the time lag τ_{ns}. A very small value of t_{sn}/τ_{ns} undervalues the time t by a factor 2 or 3 and has a negligible effect in a logarithmic scale. The first crystallization occurs when $J = (v.t_{sn})^{-1}$ in the presence of one intrinsic growth nuclei in the sample volume v. The critical energy barrier is obtained using (5) and the values of ε_{nm} as a function of θ^2; t_{sn} is deduced from (20) with $\ln(K_{ls})$ given by (3).

Assuming that the intrinsic nuclei are very numerous regardless the sample volume v, the steady-state nucleation rate J per volume unit and per second is given by:

$$\ln(J.v.t_{sn}) = \ln(K_{ls}v.t_{sn}) - \frac{\Delta G_{eff}^*}{k_B T}, \text{ where } \frac{\Delta G_{eff}^*}{k_B T} = \frac{\Delta G_{2ls}^*}{k_B T} - \frac{\Delta G_{nm}}{k_B T} \tag{20}$$

where t_{sn} is the steady-state nucleation time and ΔG_{nm} the free-energy change associated with the previous solidification of non-melted crystals [8-10,44,62]].

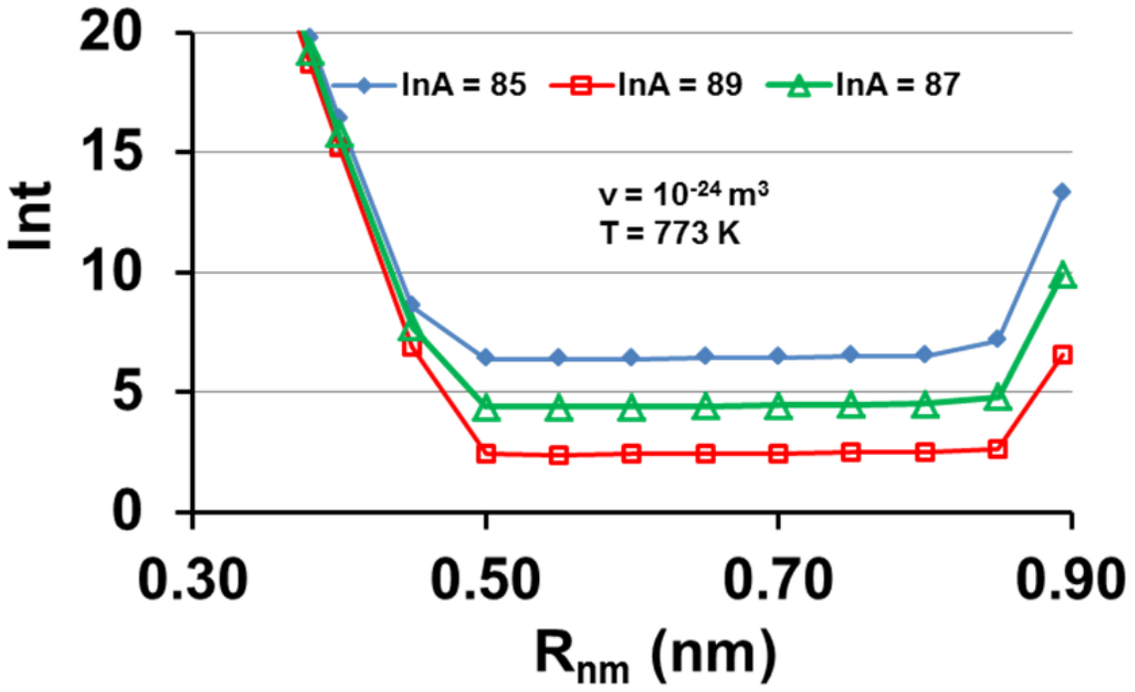

Figure 13. The logarithm of the nucleation full time t is plotted as a function of the nucleus radius R_{nm} using three values of lnA, ΔH_m = 5100 J. and the corresponding values of $\ln K_{ls}$ at Tx = 773 K. The shortest nucleation times are equal to 584, 79 and 11 s as compared to an experimental value of 600 s. This nucleation time is dominated by the transient time τ_{ns} which becomes much larger at T_g = 676 K and equal to 2×10^{18} s. These results lead to $(T_x - T_g) \cong 97$ K measured with a heating rate of 10K/mn. Similar curves are obtained using ΔH_m = 4600 J and are not represented.

The steady–state homogeneous-nucleation time t_{sn} (ΔG_{nm} = 0) necessary to observe a first crystallization would be equal to 10^{24} seconds with a sample volume v =10^{-24} m^3. The energy barrier ΔG_{nm} of intrinsic nuclei is calculated using (2); the radius R_{nm} of intrinsic nuclei is temperature-independent down to the growth temperature; $\varepsilon_{nm}(\theta)$ is assumed to vary as $\varepsilon_{ls}(\theta)$ given by (3) with ε_{ls0} replaced by ε_{nm0} which is calculated using (14-16). A unique nucleus in a volume v_s = 10^{-24} m^3 still acts as growth nucleus and produces a nano-crystallization process of the undercooled melt as shown in Figure 13.

The Bi2212 melt contains more than 10^{24} nuclei per m^3 in full agreement with nanocrystallization experiments [61]. The values of lnA are equal to 87 ± 2 as already shown for glass-forming melts having about the same T_g/T_m and V_m. The total nucleation time t is calculated by adding t_{sn} and τ_{ns} with (18). The shortest nucleation time is equal to 584, 79 and 11 s for lnA = 85, 87 and 89 respectively. The nanocrystallization has been observed at T = 773 K after 600 s in perfect agreement with the curve lnA = 85. The model developed above has already predicted the time-temperature transformation diagram of several glass-forming melts [47].

Surviving intrinsic nuclei have been called non-melted crystals. These clusters exist in the melt above T_m and they have a stability only expected in super-clusters which could correspond to a complete filling of electron shells [51,52]. This assumption might be correct if the structural change of surviving crystals in less-dense superclusters occurs without complementary Gibbs free energy. The Gibbs free energy change (12) induced by a volume increase would remain constant because it only depends on $R/(V_m/N_A)^{1/3}$. An increase of the cluster molar volume would be followed by an increase of R without change of ε_{nm0} and U_0 in (15), (16) and (8). Then, surviving intrinsic nuclei could be super-clusters already observed in liquid aluminium by high energy X-rays [55]. We develop here the idea that the super-clusters are solid residues instead of belonging to the melt structure.

The model described here also predicts the undercooling temperatures of liquid elements [64]. It only requires the knowledge of the melting temperature of each nucleus as a function of their radius, the fusion heat of a bulk multicomponent material, its molar volume, its melting temperature and its vitreous transition temperature. Adjustable parameters are not required. There is an important limitation to its use because all atoms are considered as being identical. Thus, it cannot describe the behaviour at high temperatures of clusters which have a composition strongly different from that of the melt. We did not find any publication about the existence of a vitreous state of Y123. This could be due to a much smaller viscosity of this melt. Nevertheless, this material can be magnetically textured due to the presence of intrinsic clusters above T_m. Its unknown energy saving coefficient ε_{ls0} could be smaller than 1 and could not be determined using equations only governing fragile glass-forming melts. The growth of nuclei occurs inside the temperature interval between liquidus and solidus. The magnetic field can give a direction to the free crystals when their size depending on their magnetic anisotropy is sufficiently large; the processing time below the liquidus temperature has to be adapted to their growth velocity.

4. Conclusion

Magnetic texturing experiments using pre-reacted powders of Bi2212, Bi2223 or Y123 show that crystal alignment in magnetic field is successful when the annealing temperature is slightly superior to the critical temperature T_m. This temperature corresponds to the liquidus temperature T_m above which there is no solid structure except isolated growth nuclei imbedded in the melt having radii smaller than a critical value. The growth around nuclei occurs in a window of solidification extending from T_m and leads to crystals which become free to align in the magnetic field when their anisotropy energy becomes larger than k_BT. The thermal cycle has to use an annealing temperature a little larger than T_m in order to be sure that crystallisation will start from surviving nuclei of superconducting phases and not from polycrystalline entities. The overheating temperature has to be limited to a few degrees Celsius up to a few tens of degrees above T_m depending on the amplitude of the magnetic field. This will insure that the number of nuclei per volume unit remains important and that the composition of nuclei is not progressively transformed into non-superconducting secondary phase nuclei accompanying the oxygen loss.

Short and long lengths of Bi2212 conductors obtained from pre-reacted powders of Bi2212 were textured using the same thermal cycle with a maximal annealing temperature a little larger than T_m and a relatively small annealing time. This thermal cycle is to be compared to the usual long annealing time imposed at lower temperatures in order to form the superconducting phase from non-reacted precursors. This process is successful even without magnetic field because the melt already contains surviving nuclei of this phase acting as growth nuclei inside the silver-sheathed filaments having a section sufficiently small to accommodate the platelets obtained after growth. The alignment of these platelets and consequently the superconducting critical current are improved by using a dynamic process reproducing the thermal cycle presented above where the wire moves through the magnetic field.

We have used a model which predicts glass-forming melt properties without using adjustable parameters and only knowing the fusion heat of a bulk multicomponent material, its molar volume, its melting temperature and its vitreous transition temperature T_g. The Bi2212 and Bi2223 ceramics are known to lead to a vitreous state after quenching. The knowledge of T_g leads to the homogeneous nucleation temperature of crystal and to the energy saving associated with the complementary Laplace pressure acting on a critical radius crystal which is associated with the Fermi energies equalization of this crystal and melt at all temperatures T larger than T_g. The melting temperature of each nucleus above T_m depends on its radius which is smaller than its critical value at T_m. A simple method of quantification is used to determine the complementary Laplace pressure depending on the crystal radius. This energy saving of surviving crystals is calculated assuming that the equalization of Fermi energies between crystal and melt virtually occurs by free electron transfer from crystal to melt. A bound state of a s-state electron would be produced in the electrostatic spherical potential of radius R_{nm}; the energy saving depending on R_{nm} would be equal to its first energy level. This energy is constant above T_m at constant radius and decreases with $\theta^2 = (T-T_m)^2/T_m^2$ below T_m. The transient and steady-state nucleation times of the Bi2212 nano-crystallized state are predicted in agreement with the observed values. There is a limitation to the model since we consider all atoms to be identical. Consequently, it cannot describe the behaviour at too high temperatures of clusters which have a composition strongly different from that of the melt. The model predicts that the highest melting temperature of surviving crystals occurs at $\theta = 0.93$. This value is too high because the vitreous state is obtained by quenching the melt from $\theta \cong 0.3$. In addition, Bi2212 and, Bi2223 nuclei are rapidly transformed in secondary phase clusters which govern the nano-crystallization of the melt. We did not find any publication about the existence of a vitreous state of YBCO. This could be due to a much smaller viscosity of this melt. Nevertheless, this material can be magnetically textured due to the presence of intrinsic clusters above T_m. Its unknown energy saving coefficient ε_{ls0} could be smaller than 1 and could not be determined using equations only governing fragile glass-forming melts.

Author details

Laureline Porcar, Patricia de Rango, Daniel Bourgault and Robert Tournier
Institut Néel/CRETA/CNRS/ University Joseph Fourier/Grenoble/France

Acknowledgments

The authors thank the Institute of Physics Publishing, IOP publishing, Taylor and Francis Group Journals, Elsevier for giving the authorization to reproduce Figure 1 and 2 as published in [16], Figure 4 as published in [23], Figure 6 as published in [26], Figure 7 as published in [34], Figure 8 and 9 as published in [35] and Figure 10 as published in [38].

5. References

[1] Beaugnon E, Bourgault D, Braithwaite D, de Rango P, Perrier de la Bâthie R, Sulpice et al. Material processing in high static magnetic field: a review of an experimental study of levitation, phase separation, convection and texturation. J de Physique,1993; 3:399-421.

[2] Yamaguchi M, Tanimoto Y. Magneto-Science: Magnetic Field Effects on Materials: Fundamentals and Applications. Ed: Springer Series in Materials Science vol 89, Tokyo: Kodansha. 2006.

[3] Tournier R. Method for preparing an oriented and textured magnetic material, U.S.A. Patent, 1992; Dec. 1, N° 5,168,096.

[4] Tournier R, Crystal making method. U.S.A. patent, 1993; june 8, N° 5,217,944.

[5] Tournier, RF. Presence of intrinsic growth nuclei in overheated and undercooled liquid elements. Physica B, 2007; 392:79-91.

[6] Tournier RF. Tiny crystals surviving above the melting temperature and acting as growth nuclei of the high –Tc superconductor microstructure. Mat. Sc. Forum, 2007; 546-549:1827-40.

[7] Tournier R F, Beaugnon E. Texturing by cooling a metallic melt in a magnetic field. Sci. Technol. Adv. Mater. 2009; 10:014501 (10pp), available from: URL: http://stacks.iop.org/1468-6996/10/014501.

[8] Turnbull D. Kinetics of solidification of supercooled liquid mercury droplets. J. Chem. Phys.1952; 20: 411-24.

[9] Kelton K F. Crystal nucleation in liquids and glasses, Solid State Phys. 1995; 45:75 -177.

[10] Vinet B, Magnusson L, Fredriksson H, Desré PJ. Correlations between surface and interface energies with respect to crystal nucleation. J. Coll.Interf. Sc. 2002; 255:363-374.

[11] Tong HY, Shi FG. Abrupt discontinuous relationships between supercooling and melt overheating. Appl. Phys. Lett. 1997; 70:841-43

[12] Mikelson AE, Karklin YK. Control of crystallization processes by means of magnetic fields. J. Cryst. Growth, 1981; 52:524-29

[13] Ferreira JM, Maple M B, Zhou H, Hake RR, Lee BW, Seaman CL, Kuric M V et al. Magnetic field alignment of high-Tc Superconductors $RBa_2Cu_3O_{7-\delta}$. Appl. Phys. A , 1988; 47:105-10.

[14] Lees MR, de Rango P, Bourgault D, Barbut JM, Braithwaite D, Lejay P et al. Bulk textured rare-earth-$Ba_2Cu_3O_{7-\delta}$ prepared by solidification in a magnetic field. Supercond. Sci. Technol.1992; 5:362-7.

[15] De Rango P, Lees M, Lejay P, Sulpice A, Tournier R., Ingold M et al, Texturing of magnetic materials at high temperature by solidification in a magnetic field, Nature, 1991; 349:770-1.

[16] Lees M, Bourgault D, de Rango P, Lejay P, Sulpice A, Tournier R. A study of the use of a magnetic field to control the microstructure of the high-temperature superconducting oxide $YBa_2Cu_3O_{7-\delta}$ Phil. Mag. B, 1992; 65:1395-404.

[17] Bourgault D, de Rango P, Barbut JM, Braithwaite D, Lees MR, Lejay P et al. Magnetically melt-textured $YBa_2 Cu_3O_{7-\delta}$ Physica C, 1992; 194, pp. 171-6

[18] Barbut JM, Barrault M, Boileau F, Ingold F, Bourgault D, de Rango P, Tournier R. D.C. transport current in excess 1000A in a superconducting material textured by a zone melting set-up in a magnetic field. Appl. Superc.1993; 1:345-8.

[19] Barbut JM, Bourgault D, Schopohl N, Sulpice A, Tournier R. Scaling laws Jc (H/Hc_3(◎)) and intrinsic surface superconductivity in $YBa_2 Cu_3O_{7-\delta}$. Physica C, 1994; 235-240:2995-6.

[20] Porcar L, Bourgault D, Barbut JM, Barrault M, Germi P, Tournier R. High transport currents of melt textured YBCO up to 6000 A, Physica C, 1997; 275:293-8.

[21] Tournier R, Beaugnon E, Belmont O, Chaud X, Bourgault D, Isfort D et al. Processing of large $YBa_2Cu_3O_{7-x}$ single domains for current-limiting applications. Supercond. Sci. Technol. 2000; 13:886-95.

[22] Strobel P, Korczak W, Fournier T. A thermal analysis study of the system Bi-Sr-Ca-Cu-O at variable oxygen pressure. Phys. C,1989; 161:167-74.

[23] Strobel P, Toledano JC, Morin D, Schneck J, Vacquier G, Monnereau O et al. Phase diagram of the system $Bi_{1.6}Pb_{0.4}Sr_zCuO_6$-$CaCuO_2$ between 825°C and 1100°C. Physica C, 1992; 201:27-42.

[24] Pavard S, Villard C, Bourgault D, Tournier R. Effect of adding MgO to bulk Bi2212 melt textured in a high magnetic field., Supercond. Sci. Technol. 1998; 11:1359-66.

[25] Chen WP, Maeda H, Kakimoto K, Zhang PX, Watanabe K, Motokawa M. Processing of Ag-doped Bi2212 bulks in high magnetic fields: a strong correlation between degree of texture and field strength, Physica. C, 1999; 320:96-100.

[26] Maeda H, Chen WP, Inaba T, Sato M, Watanabe K, Motokawa M. Texture development in Bi-based superconductors grown in high magnetic fields and its effect on transformation of Bi(Pb)2212 to Bi(Pb)2223, Physica C, 2001; 354:338-41.

[27] Maeda H, Sastry PVPSS, Trociewitz UP, Schwartz J, Ohya K, Sato et al. Effect of magnetic field strength in melt-processing on texture development and critical current density of Bi-oxide superconductors. Physica C, 2003; 386:115–121.

[28] Tournier R, Pavard S, Bourgault D, Villard C. Bulk Bi2212 texturing by solidification in a high magnetic field and hot forging, Int. Symp. on Superc. XII, ISS 99, Morioka, Japan,1999; pp. 527-9.

[29] Liu HB, Ferreira PJ, Vander Sande JB. Processing Bi-2212/Ag thick films under a high magnetic field: on the Bi-2212/Ag interface effect. Physica C, 1998; 303:161-168.

[30] Chen WP, Maeda H, Watanabe K, Motokawa M, Kitaguchi H, Kumakura H. Microstructures and properties of Bi 2212 Ag tapes grown in high magnetic fields. Physica C, 1999; 324:172-6.

[31] Maeda H, Ohya K, Sato M, Chen WP, Watanabe K, Motokawa M, et al. Microstructure and critical current density of Bi2212 tapes grown by magnetic melt-processing, Physica C, 2002; 382:33-7.
[32] Liu X, Schwartz J. On the influence of magnetic field processing on the texture, phase assemblage and properties of low aspect ratio Bi2Sr2CaCu2Ox/AgMg wire. Sci. Technol. Adv. Mater., 2009, 10, 014605 (11pp), available from: URL: http://stacks.iop.org/STAM/10/014605.
[33] Flahaut E, Bourgault D, Bruzek CE, Rikel MO, Herrmann P, Soubeyroux, J.-L.,et al. R. Dynamic heat treatment of BSCCO-2212 tapes with homogeneous properties and high critical current density. IEEE-Trans.-Appl.-Supercond. June 2003; 13(2) pt. 3: 3034-7.
[34] Bruzek C-E, Lallouet N, Flahaut E, Bourgault D, Saugrain J-M, Allais A et al. High performance Bi2212/Ag tape produced at Nexans. IOP Conf. Series, 2003; 181:2260-7.
[35] Villaume A, Bourgault D, Porcar L, Girard A, Bruzek CE, Sibeud PF. Misalignment angles reduction in Bi2212 multifilaments melted by dynamic heat treatment under a magnetic field. Supercond. Sci. Technol. 2007; 20:691-6.
[36] Noudem JG, Beille J, Bourgault D, Sulpice A, Tournier R. Combined effect of melting under magnetic field and hot pressing to texture superconducting ceramics Bi-Pb-Sr-Ca-Cu-O (2223). Physica C,1994; 235-240:3401-2
[37] Noudem JG, Beille J, Bourgault D, Beaugnon E, Chateigner D, Germi P et al. Magnetic melt texturation combined with hot pressing applied to superconducting ceramics Bi-Pb-Sr-Ca-Cu-O (2223). Supercond. Sc. Technol.1995; 8:558-63
[38] Noudem J, Beille J, Bourgault D, Chateigner D, Tournier R. Bulk Bi-Pb-Sr-Ca-Cu-O (2223) ceramics by solidification in a magnetic field. Physica C, 1996; 264:325-30.
[39] Giannini E, Savysyuk I, Garnier V, Passerini R, Toulemonde P, Flükiger R. Reversible melting and equilibrium phase formation of $(Bi,Pb)_2Sr_2Ca_2Cu_3O_{10+\delta}$. Supercond. Sci. Technol. 2002, 15:1577-86.
[40] Li JY, Soubeyroux J-L, Zheng HL, Li CS, Lu YF, Porcar L, Tournier R et al. Phase evolution during the melting and recrystallization of ceramic core in the (Bi,Pb)-2223 tape. Physica C, 2006; 450:56–60.
[41] Hays CC, Johnson WL. Undercooling of bulk metallic glasses processed by electrostatic levitation. J. Non-Cryst. Solids, 1999; 250-252:596-600.
[42] Fan C, Inoue A. Influence of the liquid states on the crystallization process of nanocrystal-forming Zr-Cu-Pd-Al metallic glasses. Appl. Phys.Lett. 1999; 75:3644-6.
[43] Rudolph P, Koh HJ, Shäfer N, Fukuda T. The crystal perfection depends on the superheating of the mother phase too - experimental facts and speculations on the "melt structure" of semiconductor compounds. J. Cryst. Growth, 1996; 166:578-82.
[44] Gutzow I, Schmelzer. The vitreous state. Ed : Springer, 1995.
[45] Doolittle AK. Studies in Newtonian Flow. II. The dependence of the viscosity of Liquids on Free-Space. J. Appl. Phys. 1951; 22:1471-5.
[46] Angell C. A. Formation of glasses from liquids and biopolymers, Science, 1995; 267, pp 1924-1935.
[47] Tournier RF. Crystal growth nucleation and Fermi energy equalization of intrinsic spherical nuclei in glass-forming melts. Sci. Technol. Adv. Mater. 2009; 10:014607 (12pp), available from: URL: http://stacks.iop.org/1468-6996/10/01450.

[48] Lu K, Li Y. Homogeneous nucleation catastrophe as a kinetic stability limit for superheated crystal. Phys. Rev. Lett. 1998; 80:4474-7.
[49] Jiang Q, Zhang Z, Li JC. Melting thermodynamics of nanocrystals embedded in a matrix. Acta Mater. 2000; 48:4791-5.
[50] Reedjik MF, Arsic J, Hollander F FA, De Vries SA, Vlieg E. Liquid order at the interface of KDP crystals with water: evidence for ice-like layers. Phys. Rev. Lett. 2003; 90:066103
[51] De Heer WA. The physics of simple metal clusters: experimental aspects and simple model, Rev. Mod. Phys. 1993; 65:611-76.
[52] Kulmin VI, Tytik DL, Belashchenko DK, Sirenko A N. Structure of silver clusters with magic numbers of atoms by data of molecular dynamics. Colloid J. 2008; 70:284-96.
[53] Liu R-S, Liu H-R, Dong K-J, Hou Z-Y, Tian Z-A, Peng A-B et al. Simulation study of size distributions and magic number sequences of clusters during the solidification process in liquid metal Na. J. Non-Cryst.Sol. 2009; 355:541–47.
[54] Almyras GA, Lekka CE, Mattern N, Evangelakis GA. On the microstructure of the $Cu_{65}Zr_{35}$ and $Cu_{35}Zr_{65}$ metallic glasses. Scripta Mater. 1996, 62:33-36.
[55] Mauro NA, Bendert J C, Vogt AJ, Gewin JM, Kelton KF. High energy x-ray scattering studies of the local order in liquid Al. J. Chem. Phys. 2011, 135 (4):044502-1-6.
[56] Tournier RF. Thermodynamics of vitreous transition. Revue de Métallurgie, 2012; 109:27-33.
[57] Tournier RF. Thermodynamic and kinetic origins of the vitreous transition. Intermetallics, 2012; doi:10.1016/j.intermet.2012.03.024.
[58] Ramanathan S, Li Z, Ravi-Chandar K. On the growth of BSCCO whiskers. Phys. C, 1997; 289:192-98.
[59] Tournier RF. Thermodynamic origin of the vitreous transition, Materials, 2011, 4:869-92. available from URL: http://www.mdpi.com/journal/materials
[60] Mayoral MC, Andres JM, Bona M T, Angurel L A, Natividad E. Application to the laser floating zone: preparation of high temperature BSSCO superconductors by DSC. Thermochimica Acta, 2004; 409:157-164.
[61] Müller C, Majewski P, Thurn G, Aldinger F. Processing effects on mechanical and superconducting properties of Bi 2201 and Bi 2212 glass ceramics. Phys. C, 1997; 275:337-45.
[62] Turnbull D, Fisher JC. Rate of nucleation in condensed sytems. J. Chem. Phys. 1948; 17:71-3.
[63] Tournier RF. Expected properties of gold melt containing intrinsic nuclei, Proc. 6th Intern. Conf. Electrom. Process. Mat., Dresden, Ed: Forschungszentrum Dresden-Rossendorf, Germany,2009, pp. 304-307.
[64] Tournier RF. Undercooling versus Overheating of Liquid Elements Containing Intrinsic Nuclei: Application to Magnetic Texturing. Ppt presentation at MAP4 in Atlanta, 2010, available from URL: http://creta.cnrs.fr.
[65] Landau L, Lifchitz E. Mécanique Quantique. Editions MIR, Moscou,1966 ; pp.135-136.